



OPEN

# Towards stable silicon nanoarray hybrid solar cells

SUBJECT AREAS:

SOLAR CELLS

ORGANIC-INORGANIC  
NANOSTRUCTURESW. W. He<sup>1</sup>, K. J. Wu<sup>2</sup>, K. Wang<sup>1</sup>, T. F. Shi<sup>1</sup>, L. Wu<sup>1</sup>, S. X. Li<sup>1</sup>, D. Y. Teng<sup>1</sup> & C. H. Ye<sup>1</sup>

<sup>1</sup>Anhui Key Laboratory of Nanomaterials and Technology, and Key Laboratory of Materials Physics, Institute of Solid State Physics, Chinese Academy of Sciences, Hefei 230031, China, <sup>2</sup>State Key Laboratory of Magnetic Resonance and Atomic and Molecular Physics, Wuhan Institute of Physics and Mathematics, Chinese Academy of Sciences, and Wuhan National Laboratory for Optoelectronics, Wuhan 430071, China.

Received  
26 November 2013Accepted  
18 December 2013Published  
16 January 2014

Correspondence and  
requests for materials  
should be addressed to  
C.H.Y. (chye@issp.ac.  
cn)

**Silicon nanoarray hybrid solar cells benefit from the ease of fabrication and the cost-effectiveness of the hybrid structure, and represent a new research focus towards the utilization of solar energy. However, hybrid solar cells composed of both inorganic and organic components suffer from the notorious stability issue, which has to be tackled before the hybrid solar cells could become a viable alternative for harvesting solar energy. Here we show that Si nanoarray/PEDOT:PSS hybrid solar cells with improved stability can be fabricated via eliminating the water inclusion in the initial formation of the heterojunction between Si nanoarray and PEDOT:PSS. The Si nanoarray hybrid solar cells are stable against rapid degradation in the atmosphere environment for several months without encapsulation. This finding paves the way towards the real-world applications of Si nanoarray hybrid solar cells.**

Solar energy is one of the most abundant renewable clean energy forms in our world. By photovoltaic effect, solar energy can be converted into electricity. In the past half century, we have witnessed the progress of the photovoltaic devices. Especially, one of the representative solar cells, monocrystalline Si solar cell, has reached a single cell efficiency higher than 24%<sup>1</sup>. However, the process complexity and the high cost involved in the fabrication limit the large-scale deployment of monocrystalline Si solar cells. Alternatively, organic solar cells are one of the promising solutions because of the ease of processing and the low cost<sup>2</sup>. Si-organic hybrid solar cells have been drawing more and more attention in recent years<sup>3–5</sup> and represent one of the most promising inorganic-organic hybrid solar cells, because they combine the high carrier mobility in Si and the low-cost processing of the organic materials. So far, Si/PEDOT:PSS hybrid solar cells have been reported with steady increase in efficiency over the years<sup>6–13</sup>. It is well-known that material morphology acts as an important role in improving the efficiency. In order to enhance the efficiency, the cylindrical core-shell structure has shown especially promising progress, because this structure can increase the area of the interface and facilitate the separation of excitons<sup>14–17</sup>. An efficiency higher than 10% has been achieved by several research groups<sup>3,14,17</sup>, and even an efficiency higher than 12% has been reported recently for Si/PEDOT:PSS hybrid cells on random pyramid-textured Si wafers<sup>18</sup>.

It is well documented that organic solar cells suffer from the stability issues<sup>19</sup>, that is, the performance of the organic solar cells degrades dramatically after exposed to atmospheric conditions with a normal content of oxygen and humidity level. Encapsulation of the solar cells complicates the fabrication processes and increases the production cost. Some researchers have studied the stability of organic solar cells, focusing on the organic semiconductors<sup>20</sup>, poly(3,4-ethylenedioxythiophene)/poly(styrenesulfonate) (PEDOT:PSS) hole conductors<sup>21</sup>, and the interface between PEDOT:PSS and ITO electrode<sup>22,23</sup>. They found that all the above components in the organic solar cells could lead to the degradation of the performance of organic solar cells. It is rather surprising that there have only limited reports on the stability investigation of Si/PEDOT:PSS hybrid solar cell<sup>18</sup>, although this hybrid solar cells also contain PEDOT:PSS and sometimes PEDOT:PSS/ITO interfaces, and also poses the same stability issues. In this work, we find that the performance of Si nanoarray (SiNA)/PEDOT:PSS hybrid solar cells fabricated following the literature recipe indeed degrades substantially with time in the atmospheric environment. We find that water trapped in the process of PEDOT:PSS deposition dramatically affects the quality of the heterojunctions between SiNAs and PEDOT:PSS. As long as we eliminate the water content immediately after the deposition of PEDOT:PSS, the stability of SiNA/PEDOT:PSS hybrid solar cells is improved dramatically in the environment humidity. This finding opens the door to the real-world application of SiNA/PEDOT:PSS hybrid solar cells.

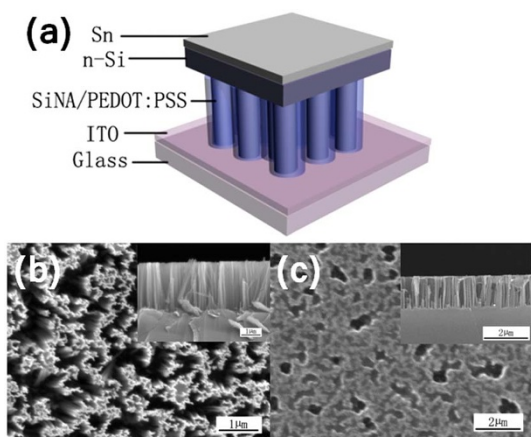


**Figure 1** | SiNA/PEDOT:PSS hybrid solar cells. (a) Schematic illustration of SiNA/PEDOT:PSS hybrid solar cells. (b) Top-view SEM image of SiNA. (c) Top view SEM image of SiNAs embedded with PEDOT:PSS. Insets in (b) and (c) are cross-sectional view SEM images.

## Results

The structure of the hybrid solar cell is schematically illustrated in Figure 1a. SiNAs were prepared by metal-assisted chemical etching and are exhibited in Figure 1b. We fabricated SiNA/PEDOT:PSS hybrid solar cells following the literature recipe<sup>15,24</sup>, by impressing SiNAs on PEDOT:PSS-coated ITO substrates, followed by a natural drying in a glove box for 12 h to form the heterojunction between SiNAs and PEDOT:PSS. Before the assembly of the cells, drying at 140°C for 1 h was applied (labeled as cell 1 if not stated otherwise). We found that the performance of the solar cells degraded substantially when the cells were illuminated with AM 1.5 solar simulator (Figure 2a). To elucidate the origin of the rapid degradation of the performance of the cells, we proposed a recipe for the assembly of the cells. Instead of impressing SiNAs on wet PEDOT:PSS films, we first coated PEDOT:PSS on SiNAs via doctor-blading, and then dried the PEDOT:PSS film in the glovebox for 12 h and then heated on a hot plate at 120°C for 5 min. After drying, SiNAs were embedded with PEDOT:PSS (Figure 1c). We then laminated PEDOT:PSS-coated SiNA and PEDOT:PSS-coated ITO substrates to assemble the cells following a drying at 140°C for 1 h (labeled as cell 2 if not stated otherwise). The cells fabricated with this recipe did not show pronounced degradation under illumination (Figure 2b).

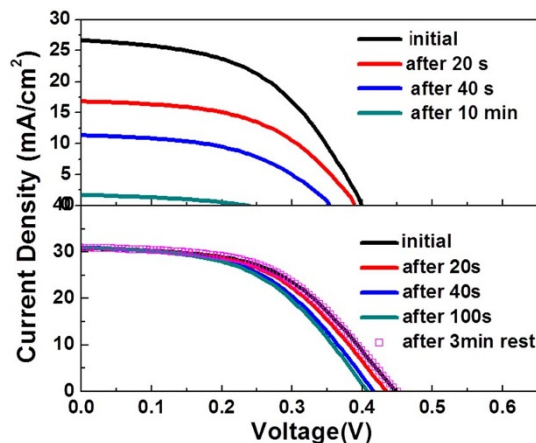


**Figure 2** | Stability of SiNA/PEDOT:PSS hybrid solar cells. *J*-*V* curves of SiNA/PEDOT:PSS hybrid solar cell fabricated following the literature recipe (cell 1, upper panel). (b) *J*-*V* curves of SiNA/PEDOT:PSS hybrid solar cells fabricated by our new recipe (cell 2, bottom panel).

It seems that the main difference of the two recipes is the drying of PEDOT:PSS film interfaced with SiNA in our recipe. Therefore, we suspect that the heterojunction between the wet PEDOT:PSS film and SiNAs may undergo degradation or structure variation under illumination. It is not surprising that the performance-degraded solar cells could partially recover after a post-drying process (Figure 3) (labeled as cell 3 if not stated otherwise). After recovery, the stability of cell 3 was also improved. To further study the stability of the solar cell (cell 2) in the environment atmosphere under long term storage without encapsulation, we found that the cell showed an average efficiency loss  $\sim 45\%$  (from 7.7% to 4.2%) during a period of five months (Figure 4). The open-circuit voltage ( $V_{oc}$ ) and the short-circuit current density ( $J_{sc}$ ) only exhibited a slight average decrease of  $\sim 9\%$  from 0.46 V to 0.42 V and  $\sim 12\%$  from 25 mA/cm<sup>2</sup> to 22 mA/cm<sup>2</sup>, respectively. The fill factor (FF) exhibited an average decrease of  $\sim 26\%$ .

We measured the temperature increase of the solar cells under the illumination of the solar simulator and plotted the data of  $V_{oc}$ ,  $J_{sc}$ , FF, and  $\eta$  of cell 1 and cell 2 in Figure 5. Besides the reduction of  $V_{oc}$  from 0.40 V to 0.23 V, we can see a dramatic reduction of  $J_{sc}$  from 26 to 2 mA/cm<sup>2</sup> for cell 1, in sharp contrast to the constancy of  $J_{sc}$  for cell 2 (a slight decrease of  $V_{oc}$  from 0.45 V to 0.42 V and a slight increase of  $J_{sc}$  from 27 to 30 mA/cm<sup>2</sup>, respectively). In Figure 6, we plotted the reverse saturated current  $I_s$ , the photocurrent  $I_{ph}$ , the series resistance  $R_s$ , the shunt resistance  $R_{sh}$ , and the ideality factor  $n$ . Indeed, we see that  $R_s$  increases dramatically from 75 to 450  $\Omega$  for cell 1. In principle, for crystalline Si solar cells,  $J_{sc}$  generally slightly increases with temperature<sup>25</sup>. The decrease of  $J_{sc}$  with light illumination for cell 1 implies that there must something wrong with the light harvesting, the charge carrier separation, or the charge transport in the cells. Considering that SiNAs are the main light absorber, the light harvesting efficiency should not change much under light illumination. Therefore, either the interface between SiNAs and PEDOT:PSS changed in the presence of water under illumination, or the conduction of PEDOT:PSS layer degraded. We independently measured the sheet resistance of PEDOT:PSS film in the wet as well as in the dry status, and found that the conduction of dry PEDOT:PSS film was better than that of wet one (Figure S1). Upon a thorough heating, the PEDOT:PSS film exhibited a constant sheet resistance. Therefore, the larger  $R_s$  for cell 1 could be attributed to the wet PEDOT:PSS in cell 1. For example, Dupont and coworkers<sup>26</sup> reported the loss of decohesion in PEDOT:PSS when the hydrogen bonds were broken in the presence of water molecules. We noted that Shen *et al.* indeed found that post-annealing PEDOT:PSS under different atmosphere affected the conductivity of PEDOT:PSS<sup>27</sup>. The increase of  $R_s$  after heating for cell 1 has to be related to the variation at the interface between SiNA and

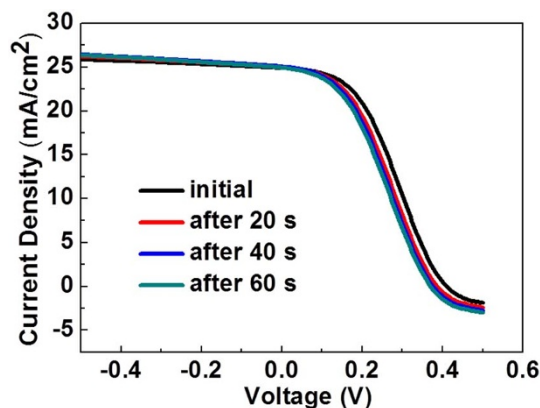


**Figure 3** | Recovery of the performance of SiNA/PEDOT:PSS hybrid solar cells. After storage of cell 1 in dry air environment for 15 days, the cell becomes stable against degradation under illumination (cell 3).

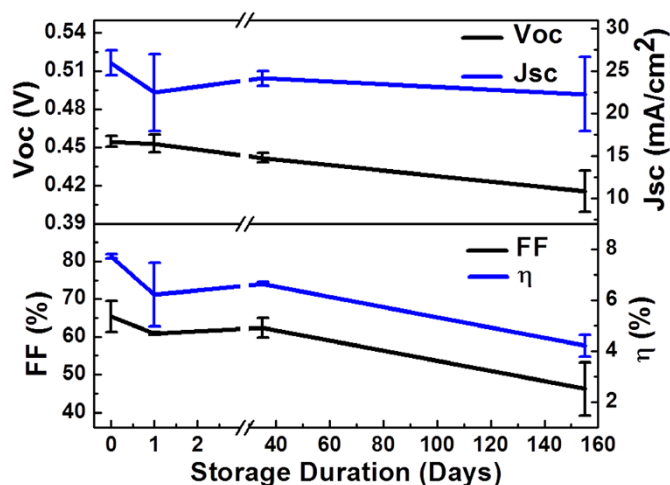


**Figure 4** | Stability of SiNA/PEDOT:PSS hybrid solar cells. Cell 2 was stored in air environment without encapsulation, and measured after different duration of storage days.

PEDOT:PSS. Through a systematic investigation, Vitoratos and coworkers<sup>28</sup> concluded that the increase of conductivity of PEDOT:PSS due to the thermal activation of the carriers and the improvement of the crystallinity competing with the decrease of conductivity resulting from the irreversible structural degradation of the polymer chains promoted by the oxygen and moisture in the atmosphere. As we noted that  $R_{sh}$  also increased for cell 1, in contrast to the constancy for cell 2, we can reach the conclusion that there must be an structural variation at the interface between SiNA and PEDOT:PSS for cell 1, which is supported by the observation of Pudasaini and coworkers that PEDOT:PSS tended to promote the formation of oxide layer on the surface of SiNAs, especially in the presence of water molecules<sup>29</sup>. It is noteworthy that the performance of the solar cells fabricated without a proper drying process can only recover to some extent after post-drying (cells 3), however, the

performance is still lower than that of the solar cells fabricated with a proper drying process as suggested in our recipe. This observation implies that although the post-drying process could remove most of the residual water molecules trapped in the deposition of PEDOT:PSS films, some irreversible chemical/physical consequences have already been generated that limit the highest achievable efficiency of the solar cells. The structural variation of cell 1 at the interface might induce defects or surface states that cause electrical variation. In a recent paper, Schmidt and coworkers<sup>18</sup> suggested the charge trapping at the interface between PEDOT:PSS and Si during the interaction with water molecules. Either the light illumination or the temperature effect will enhance the charge trapping because of the generation of more free charges. The excessive trapped charges will cause a lowering of the barrier height owing to the image charge effect<sup>30,31</sup>, which will increase the tunneling current, accounting for the faster increase of the reverse saturated current for cell 1 than for cell 2.

To further clarify the electrical variation of different cells, we used the electrochemical impedance spectroscopy (EIS) to study the solar cells, especially the interfacial structures. Nyquist, Mott-Schottky (MS), and Bode plots of the impedance spectra are displayed (Figure 7). Figure 7a exhibits the Nyquist plots of cell 1 and cell 2. It is evident that cell 1 possesses a larger series resistance than cell 2. However, the recombination resistance of cell 2 is larger than that of cell 1. Moreover, a new arc at low frequency appeared for cell 1, which was also manifested in the Bode plot of the phase angle versus frequency (Figure 7d). This new arc (or new peak in phase angle curve) indicated a new electrical process with a certain time constant. The Bode plot in Figure 7c of the modulus of the impedance also provided the same information on the appearance of a new RC component: a new platform in the curve. This observation implies that the interface between SiNA and PEDOT:PSS for cell 1 deviated dramatically from the ideal Schottky junction. There must be other conducting channels other than the normal Schottky diode appeared for cell 1. It is most possible that there are patches of varying height of Schottky barrier formed at the interface of cell 1<sup>30,31</sup>, because of the extensive trapping of charge carriers for cell 1 lowers the barrier height through

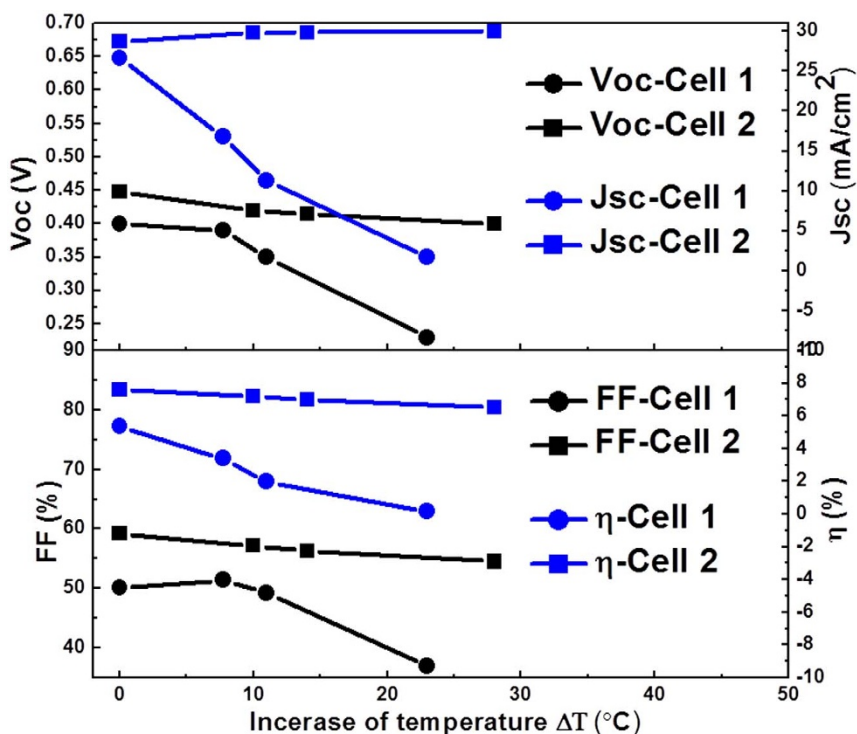


**Figure 5** | Temperature effect on the performance of SiNA/PEDOT:PSS hybrid solar cells. Variation of Voc, Jsc, FF, and η for cell 1 and cell 2.

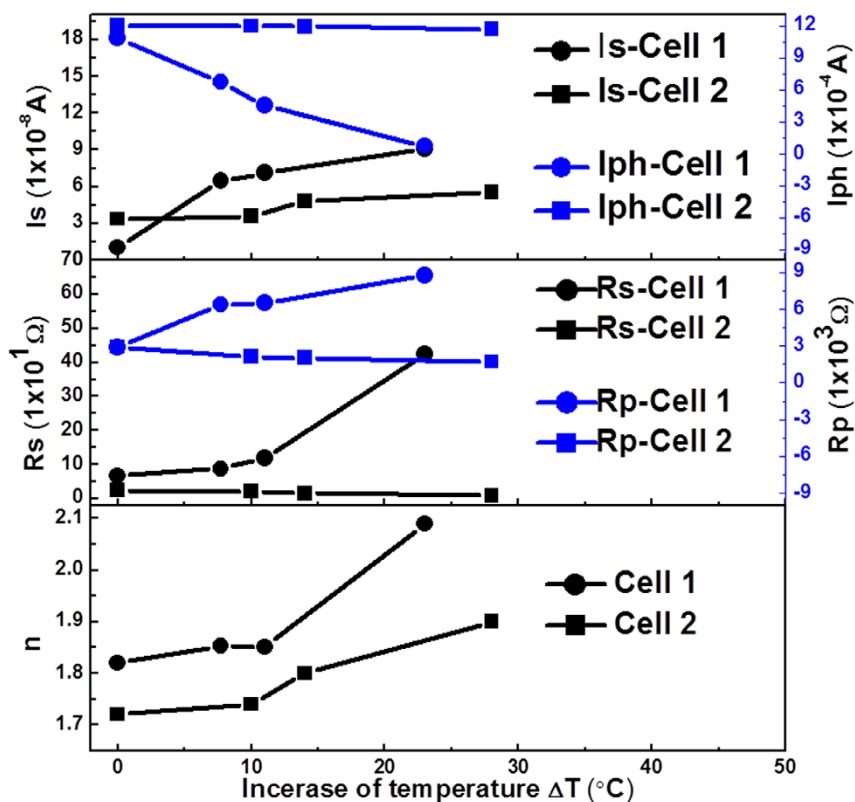


Figure 6 | Temperature effect on the performance of SiNA/PEDOT:PSS hybrid solar cells. Variation of  $I_s$ ,  $I_{ph}$ ,  $R_s$ ,  $R_{sh}$ , and  $n$  for cell 1 and cell 2.

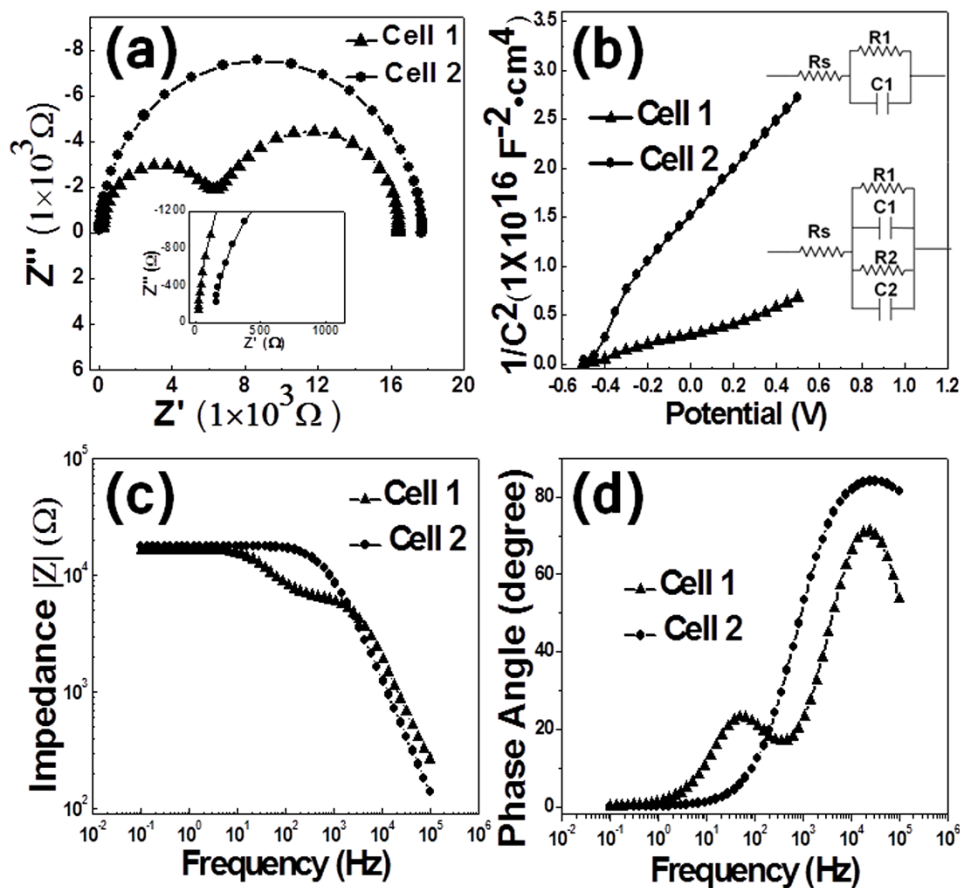


Figure 7 | Electrochemical impedance spectroscopy of SiNA/PEDOT:PSS hybrid solar cells. (a) Nyquist, (b) MS, (c) and (d) Bode plots for SiNA/PEDOT:PSS hybrid solar cells. Inset in (a) is an enlarged section at high frequency of the curves. Inset in (b) are the equivalent circuit of cell 1 and cell 2.



the image charge effect. The lowered barrier height contributed to an increased majority carrier charge transfer rate which deteriorates the performance of the solar cells<sup>32</sup>. Therefore, the barrier lowering at the patches introduced the new  $RC$  component. The excessive charge carriers for cell 1 than for cell 2 were also reflected from the larger slope of the MS plot for the latter in Figure 7b. It is interesting that even though there are patches of varying barrier height, the average barrier height did not differ much as the intercept at the potential axis is close for these two cells. The invariance of the average barrier height for cell 1 and cells 2 and the observation of  $V_{oc}$  of only 0.4–0.5 V indicate a Fermi level pinning at the interface because of the high density of interfacial states<sup>33</sup>. Without a proper interface passivation with either a well-defined oxide layer or an organic layer, the Fermi level pinning could not be removed effectively, which is however beyond the scope of this work.

In addition, we fitted the impedance curves of cell 1 and cell 2 respectively, and plotted  $R_s$ ,  $R_1$ ,  $R_2$ ,  $C_1$ , and  $C_2$  against the applied voltage in Figure 8. We can see from Figure 8a that the series resistance of both cell 1 and cell 2 does not vary much with the applied potential. The recombination resistance of both cell 1 and cell 2 decreases exponentially with the applied potential (Figure 8b) and the chemical capacitance of these two cells increases exponentially with the applied potential (Figure 8d). For cell 1, the low frequency component shows a similar magnitude of resistance to the high frequency one (Figure 8c), whereas a larger capacitance than the high frequency one (Figure 8e). The larger capacitance of the new  $RC$  component at low frequency for cell 1 agrees well to the suggestion of excessive charge trapping for cell 1. The origin of the charge trapping might come from the generation of interfacial defect patches for cell 1 because of the complicated etching behavior of PEDOT:PSS to Si/SiO<sub>x</sub> or degradation of PEDOT:PSS at the interface under illumination. In-depth investigation of the formation process and the physical nature of the defects entail further study.

## Discussion

Temperature increase in the solar cells under illumination usually causes the reduction of the open-circuit voltage ( $V_{oc}$ ). For crystalline Si solar cells,  $V_{oc}$  decreases at a rate of 2.3 mV/K<sup>24</sup>. For cell 1, we plotted the reduction of  $V_{oc}$  with the measured temperature increase

$\Delta T$  in the cells, in comparison with the theoretically calculated reduction (Figure S2, upper panel). We found that the reduction caused by temperature elevation could not account for the total decrease of  $V_{oc}$  for cell 1 (0.03 V for the calculated value versus 0.18 V for the measured value), which means that other factors have to be considered to explain the reduction of  $V_{oc}$  with illumination. In sharp contrast, cell 2 and cell 3 showed only a slight reduction of  $V_{oc}$  (0.01–0.03 V) with temperature elevation under illumination, and the measured reduction of  $V_{oc}$  could be attributed to the temperature effect (Figure S2, middle and bottom panels). It is noticed that heating actually has also a positive effect on  $V_{oc}$  because of the decrease of  $R_s$  for cell 2 as shown in the previous sections. To further prove that the temperature-induced reduction of  $V_{oc}$  for our cells, after several measurements with continuous illumination, we shut down the light source to allow the recovery of the temperature of cell 2, and 3 min later, we found that  $V_{oc}$  recovered (Figure 2b). Together with the stability of  $J_{sc}$ , we are able to unambiguously assign the reduction of  $V_{oc}$  for cell 2 and cell 3 to the temperature effect.

Recently, Schmidt and coworkers<sup>29</sup> observed a perfect stability of Si/PEDOT:PSS solar cells stored in a dessicator, whereas a drastic degradation of the efficiency from 11% to below 1% was observed in air environment within two months. However, our cells still attained more than 50% of the initial efficiency in air environment for more than five months. We, therefore, reach the conclusion that residual water molecules after deposition of PEDOT:PSS film dramatically influence the quality of the heterojunctions between SiNAs and PEDOT:PSS films, which directly affects the stability of the cells. Our experiments also demonstrate that as long as a proper heating process was applied to eliminate water molecules in PEDOT:PSS films, further uptake of water molecules from the environment was rather slow, because of the strong bonding of PEDOT:PSS grains in the film. This statement is substantiated with the performance stability of SiNA/PEDOT:PSS solar cells fabricated with our recipe. In addition, we have not found a large decrease of the conductivity of PEDOT:PSS films left in air environment after several months. Interestingly, Rivnay and coworkers<sup>34</sup> also found that the hole mobility in PEDOT:PSS films did not seem to suffer much from the uptake of water, because the cross-linking of the film reduced the uptake of water. Therefore, the poor stability of cell 1 is mainly due to the poor

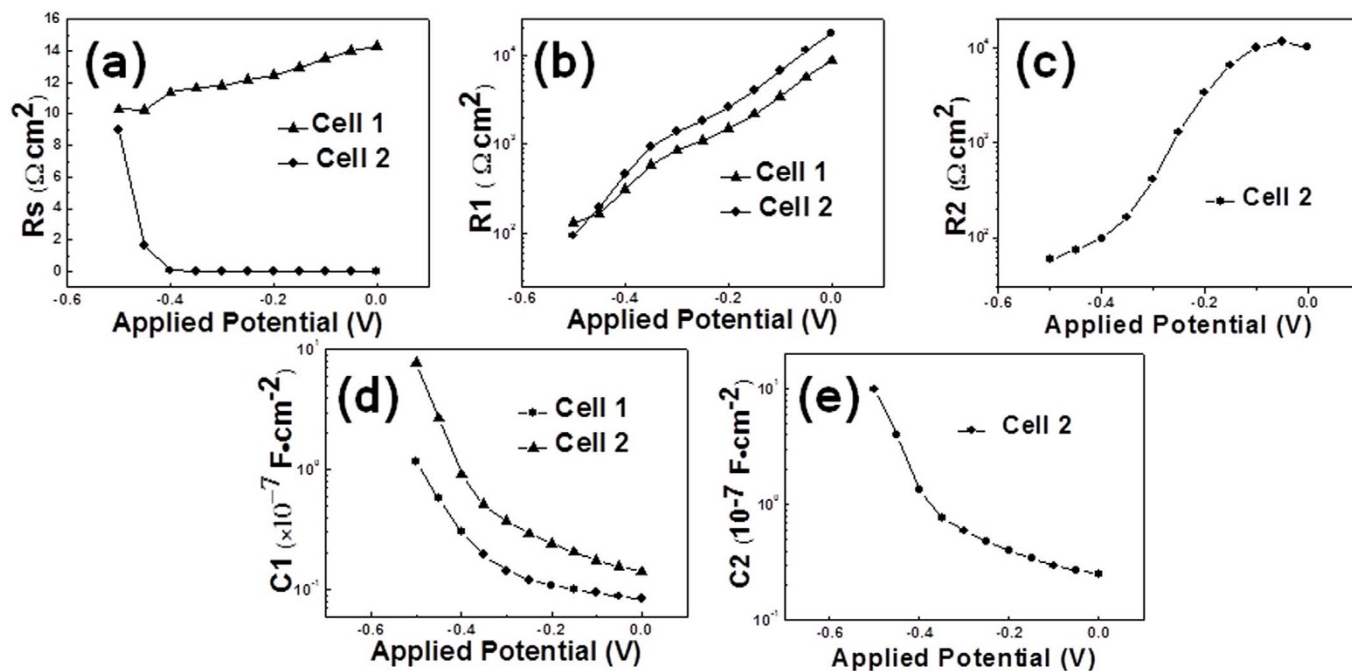


**Figure 8** | Interface electrical characteristics of SiNA/PEDOT:PSS hybrid solar cells. Variation of  $R_s$  (a),  $R_1$  (b),  $R_2$  (c),  $C_1$  (d) and  $C_2$  (e) with the applied potential for cell 1 and cell 2.



quality of the heterojunctions between SiNAs and PEDOT:PSS films caused by the inclusion of water during the deposition of PEDOT:PSS film after an insufficient drying process. Regarding the residual water in the cell after a heating process or the slight water uptake in the long-term storage process that caused the gradual loss of efficiency, it is still not clear if the interface between ITO and PEDOT:PSS plays a role, which should be investigated in further work.

In conclusion, we have proposed a recipe to prepare SiNA/PEDOT:PSS solar cells with much improved stability. We found that water inclusion in the fabrication processes of the solar cells would deteriorate the quality of the heterojunction between SiNAs and PEDOT:PSS films, which was the most important factor that caused the rapid degradation of the performance of SiNA/PEDOT:PSS solar cells. Under illumination, the degradation process was accelerated, and irreversible physical/chemical consequences happened in the interface between SiNA and PEDOT:PSS. Patches of varying Schottky barrier height owing to excessive charge trapping and the image charge lowering effect induced additional charge transfer channel, and additional arc was found in the impedance curve. The additional loss channel at the interface is the main origin for the rapid performance degradation of SiNA/PEDOT:PSS solar cells. With our proper design of the fabrication processes, SiNA/PEDOT:PSS solar cells with much improved stability could be achieved.

## Methods

**Cleaning of silicon.** The 1–10  $\Omega$ -cm n-type Si wafers were cut into area of 1x1 cm<sup>2</sup>. The substrates were successively ultrasonically cleaned for 20 min in acetone, ethanol, and solution A (1 : 1 : 4 NH<sub>3</sub>OH: H<sub>2</sub>O<sub>2</sub>: DI water), and further cleaned with deionized water and dried with N<sub>2</sub> blow.

**Preparation of SiNAs.** The clean silicon substrates were immersed in solution B (4.6 M HF and 0.02 M AgNO<sub>3</sub>) at 50°C for 3 min. After cleaned by DI water the substrates were immersed in nitric acid for 30 min to remove the silver, and then cleaned with deionized water and dried with N<sub>2</sub> blow.

**Fabrication of SiNAs/PEDOT:PSS heterojunction.** After washed by DI water, the prepared SiNAs were dipped in 2% Hydrogen fluoride (HF) solution for 1 min to remove the oxide on the surface. We put the wet SiNAs into a glove box to dry naturally. The dry SiNAs were taken out, and coated a layer of solution C (1 : 2 PEDOT:PSS: ethanol) by doctor blading method. We then spin-coated a thin layer of PEDOT:PSS containing 6% glycerol on a piece of ITO. For cell 1, we directly pressed these two parts together, and left in the glove box for 12 h for natural drying. For cell 2, we put the SiNAs and the ITO with PEDOT:PSS into the glove box for 12 h to dry naturally. Then, these two parts were heated at 120°C for 5 min at the atmosphere. Then we laminated these two parts with a layer of PEDOT:PSS containing 6% glycerol. Samples were again dried in the glove box for 12 h. We used two post-drying methods on the performance-degraded solar cell (cell 1) to recover the performance (cell 3). The first one is an accelerated drying process, where heating at 140°C for 3 h was performed. The second one is a natural drying process, where cell 1 was simply left in a desiccator for a number of days at room temperature.

**Assembly of the hybrid solar cells.** The substrates with the heterojunction structure was dried at 140°C for 1 h in the oven. The back surface of the Si substrate was etched to remove natural oxide layer. Tin was used to make the back electrode with Si by ultrasonic welding. Copper wire was attached to ITO with silver paste. The cells were baked in the oven at 140°C for 1 h.

**Characterization.** To characterize the SiNA/PEDOT:PSS structure, transmission electron microscopy (TEM, JEM 2010) and field-emission scanning electron microscope (SEM, FEI Sirion 200) imaging were performed. The cells were illuminated using a solar simulator (Oriol 3A) at one sun (AM 1.5, 100 mW cm<sup>-2</sup>), and the *J-V* characteristics were measured by using a Keithley 2400 electrometer. The temperature of the cells under illumination was measured by non-contact thermometer (Fluke 59) after each measurement of the *J-V* curves (~30 s). Electrochemical impedance spectroscopy (EIS) was carried out on an electrochemical workstation (IM6ex, Zahner).

- Zhao, J., Wang, A., Green, M. A. & Ferrazza, F. 19.8% efficient “honeycomb” textured multicrystalline and 24.4% monocrystalline silicon solar cells. *Appl. Phys. Lett.* **73**, 1991–1993 (1998).
- Service, R. Outlook brightens for plastic solar cells. *Science* **332**, 293 (2011).
- Sone, T., Lee, S. T. & Sun, B. Q. Prospects and challenges of organic/group IV nanomaterial solar cells. *J. Mater. Chem.* **22**, 4216–4232 (2012).
- Weickert, J., Dunbar, R. B., Hesse, H. C., Wiedemann, W. & Schmidt-Mende, L. Nanostructured organic and hybrid solar cells. *Adv. Mater.* **23**, 1810–1828 (2011).
- Liu, Q., Ono, M., Tang, Z., Ishikawa, R. & Ueno, K. Highly efficient crystalline silicon/zonyl fluorosurfactant-treated organic heterojunction solar cells. *Appl. Phys. Lett.* **100**, 183901 (2012).
- Jeong, S. et al. Hybrid silicon nanocone-polymer solar cells. *Nano Lett.* **12**, 2971–2976 (2012).
- He, L., Rusli, Jiang, C., Wang, H. & Lai, D. Simple approach of fabricating high efficiency Si nanowire/conductive polymer hybrid solar cells. *IEEE Electron Device Lett.* **32**, 1406–1408 (2011).
- Syu, H. J., Shiu, S. C. & Lin, C. F. Silicon nanowire/organic hybrid solar cell with efficiency of 8.4%. *Sol. Energy Mater. Sol. C.* **98**, 267–272 (2012).
- Chen, J. Y., Yu, M. H., Chang, S. F. & Sun, K. W. Highly efficient poly(3,4-ethylenedioxythiophene):Poly(styrenesulfonate)/Si hybrid solar cells with imprinted nanopyramid structures. *Appl. Phys. Lett.* **103**, 133901 (2013).
- Shiu, S., Chao, J. J., Hung, S. C., Yeh, C. L. & Lin, C. F. Morphology dependence of silicon nanowire/Poly(3,4-ethylenedioxythiophene):Poly(styrenesulfonate) heterojunction solar cells. *Chem. Mater.* **22**, 3108–3113 (2010).
- He, L., Lai, D., Wang, H. & Jiang, C. Rusli High-efficiency Si/polymer hybrid solar cells based on synergistic surface texturing of Si nanowires on pyramids. *Small* **8**, 1664–1668 (2012).
- Zhang, Y. F. et al. Heterojunction with organic thin layers on silicon for record efficiency hybrid solar cells. *Adv. Energy Mater.* DOI: 10.1002/aenm.201300923 (2013).
- Wei, W. R. et al. Above-11%-efficiency organic-inorganic hybrid solar cells with omnidirectional harvesting characteristics by employing hierarchical photon-trapping structures. *Nano Lett.* **13**, 3658–3663 (2013).
- Tsai, S. H. et al. Significant efficiency enhancement of hybrid solar cells using core-shell nanowire geometry for energy harvesting. *ACS Nano* **5**, 9501–9510 (2011).
- Lu, W. H., Wang, C. W., Yue, W. & Chen, L. W. Si/PEDOT:PSS core/shell nanowire arrays for efficient hybrid solar cells. *Nanoscale* **3**, 3631–3634 (2011).
- Adachi, M. M., Anantram, M. P. & Karim, K. S. Core-shell silicon nanowire solar cells. *Sci. Rep.* **3**, 1546 (2013).
- He, L., Jiang, C., Rusli, Lai, D. & Wang, H. Highly efficient Si-nanorods/organic hybrid core-sheath heterojunction solar cells. *Appl. Phys. Lett.* **99**, 021104 (2011).
- Schmidt, J., Titova, V. & Zielke, D. Organic-silicon heterojunction solar cells: open-circuit voltage potential and stability. *Appl. Phys. Lett.* **103**, 183901 (2013).
- Jørgensen, M. et al. Stability of polymer solar cells. *Adv. Mater.* **24**, 580–612 (2012).
- Jørgensen, M., Norrman, K. & Krebs, F. C. Stability/degradation of polymer solar cells. *Sol. Energy Mater. Sol. C.* **92**, 686–714 (2008).
- Knupfer, M. & Peisert, H. Electronic properties of interfaces between model organic semiconductors and metals. *phys. stat. sol. (a)* **201**, 1055–1074 (2004).
- de Jong, M. P., van Ijzendoorn, L. J. & de Voigt, M. J. A. Stability of the interface between indium-tin-oxide and poly(3,4-ethylenedioxythiophene)/poly(styrenesulphonate) in polymer light-emitting diodes. *Appl. Phys. Lett.* **77**, 2255–2257 (2000).
- Wong, K. W. et al. Blocking reactions between indium-tin oxide and poly(3,4-ethylene dioxythiophene):poly(styrene sulphonate) with a self-assembly monolayer. *Appl. Phys. Lett.* **80**, 2788–2790 (2002).
- Huang, J. S., Hsiao, C. Y., Syu, S. J., Chao, J. J. & Lin, C. F. Well-aligned single-crystalline silicon nanowire hybrid solar cells on glass. *Sol. Energy Mater. Sol. C.* **93**, 621–624 (2009).
- Luque, A. & Hegedus, S. John Wiley & Sons Ltd, England *Handbook of Photovoltaic Science and Engineering*. **106** (2003).
- Dupont, S. R., Novoa, F., Voroshazi, E. & Dauskardt, R. H. Decohesion kinetics of PEDOT:PSS conducting polymer films. *Adv. Funct. Mater.* DOI: 10.1002/adfm.201302174 (2013).
- Shen, X., Zhu, Y., Song, T., Lee, S. T. & Sun, B. Hole electrical transporting properties in organic-Si schottky solar cell. *Appl. Phys. Lett.* **103**, 013504 (2013).
- Vitoratos, E., Sakkopoulos, S., Paliatsas, N., Emmanouil, K. & Choulis, S. A. Conductivity degradation study of PEDOT:PSS films under heat treatment in helium and atmospheric air. *Open J. Org. Polymer Mater.* **2**, 7–11 (2012).
- Pudasaini, P. R. et al. High efficiency hybrid silicon nanopillar–polymer solar cells. *ACS Appl. Mater. Interfaces* **5**, 9620–9627 (2013).
- Werner, J. H. & Güttler, H. H. Barrier inhomogeneities at Schottky contacts. *J. Appl. Phys.* **69**, 1522–1533 (1991).
- Sawada, T. et al. Electrical properties of metal/GaN and SiO<sub>2</sub>/GaN interfaces and effects of thermal annealing. *Appl. Surf. Sci.* **159–160**, 449–455 (2000).
- Price, M. J., Foley, J. M., May, R. A. & Maldonado, S. Comparison of majority carrier charge transfer velocities at Si/polymer and Si/metal photovoltaic heterojunctions. *Appl. Phys. Lett.* **97**, 083503 (2010).
- Chen, T.-G., Huang, B.-Y., Chen, E.-C., Yu, P. C. & meng, H.-F. Micro-textured conductive polymer/silicon heterojunction photovoltaic devices with high efficiency. *Appl. Phys. Lett.* **101**, 033301 (2012).
- Rivnay, J., Owens, R. M. & Malliaras, G. G. The rise of organic bioelectronics. *Chem. Mater.* DOI: 10.1021/cm4022003 (2013).

## Acknowledgments

This work was supported by National Basic Research Program of China (973 Program, Grant No. 2011CB302103), National Natural Science Foundation of China (Grant Nos. 11274308), and the Hundred Talent Program of the Chinese Academy of Sciences.



### Author contributions

W.W.H. and C.H.Y. designed the experiments, W.W.H., K.W. and T.F.S. fabricated the devices, W.W.H., L.W., S.X.L. and D.Y.T. characterized the materials and devices, K.J.Wu did the simulation, W.W.H. and C.H.Y. analyzed the results and wrote the manuscript.

### Additional information

Supplementary information accompanies this paper at <http://www.nature.com/scientificreports>

**Competing financial interests:** The authors declare no competing financial interests.

**How to cite this article:** He, W.W. *et al.* Towards stable silicon nanoarray hybrid solar cells. *Sci. Rep.* 4, 3715; DOI:10.1038/srep03715 (2014).



This work is licensed under a Creative Commons Attribution-NonCommercial-NoDerivs 3.0 Unported license. To view a copy of this license, visit <http://creativecommons.org/licenses/by-nc-nd/3.0>